

CURL-GRADIENT IMAGE WARPING

Introducing Deformation Potentials for Medical Image Registration using Helmholtz Decomposition

Michael Sass Hansen, Rasmus Larsen

Department of Informatics and Mathematical Modelling, Technical University of Denmark, Copenhagen, Denmark

Niels Vargaard Christensen

Institute of Mathematics, University of Copenhagen, Copenhagen, Denmark

Keywords: Image registration, Morphometry, Helmholtz decomposition.

Abstract: Image registration is becoming an increasingly important tool in medical image analysis, and the need to understand deformations within and between subjects often requires analysis of obtained deformation fields. The current paper presents a novel representation of the deformation field based on the Helmholtz decomposition of vector fields. The two decomposed potential fields form a curl free field and a divergence free field. The representation has already proven its worth in fluid modelling and electrostatics, and we show it also has desirable features in image registration and morphometry in particular. The potentials are shown to offer decoupling of the two potential fields in both elastic and fluid image registration. For morphometry applications, we show that when decomposing the deformation field in symmetric and antisymmetric parts, the vector potential alone describes the vorticity, and the scalar gradient potential gives a first-order approximation to the determinant of the Jacobian. We provide some insight into the behavior of curl and divergence representation of the warp field by constructed examples and by a demonstration on real medical image data. Our theoretical findings are readily observable in our empirical experiment, which further illustrates the benefit of the parametrization.

1 INTRODUCTION

Image registration is becoming an increasingly important tool in medical image analysis, and the need to understand deformations within and between subjects often requires analysis of obtained deformation fields (Studholme and Cardenas, 2007; Davatzikos et al., 1996).

The image registration task has been approached in many different ways. It can be achieved by calculation of dense deformation fields using nonparametric methods as described by Modersitzki (Modersitzki, 2004). Vermuri *et al.* proposed a levelset representation of the deformations (Vemuri et al., 2003). For more than a decade parametric representation of the deformation fields has also been very popular in the literature, where two prominent examples are the cosine kernels presented by Cootes *et al.* (Cootes et al., 2004), and the Cubic B-spline kernels used by Rueck-

ert *et al.* (Rueckert et al., 2003). The later introduces a certain smoothing by the finite size of the parametric kernel functions, but often further *regularization* is introduced. Haber and Modersitzki introduced regularization terms to ensure displacement regularity (Haber and Modersitzki, 2007). Elastic registration is a popular form of regularization, originating from continuum mechanics as described by Christensen and Johnson (Christensen et al., 1997) and by Kybic *et al.* (Kybic and Unser, 2003).

In the subsequent morphometry it has been shown that the Jacobian of the deformation field is very important under a Gaussian random field assumption on the deformation field (Joshi, 1997). Chung *et al.* have investigated different measures of morphometry, and also introduced a strain-curl representation of the deformation field, which has interesting relations to other morphometry measures (Chung et al., 2001). Hsiao *et al.* have shown that using a parame-

terizing of the deformation field by its divergence and curl makes it less prone to grid folding than B-spline representation, while it allows for an efficient and stable optimization (Hsiao et al., 2008). Kohlberger *et al.* have used potential functions for motion estimation of fluids (Kohlberger et al., 2003).

In Section 2 we propose a new parametric representation of the deformation field, which is based on the Helmholtz decomposition of vector fields. In the following we show how this representation can also be parameterized by smooth kernels, how it can be considered a natural representation for elastic image registration, we show how it can be given a strong interpretation in morphometry, and finally we point out how the numerical stability and smoothness obtained by Hsiao *et al.* (Hsiao et al., 2008) can also be reached by our representation.

We have demonstrated an implementation of the presented method on MRI Corpus Callosa images from the midsagittal plane in Section 3.

2 METHODS

We present the developed methodology by introducing the Helmholtz decomposition representation in Section 2.1, with some intuitive demonstration of the introduced potential functions. Subsequently we give theoretical motivations by formulating simple elasticity regularization in Section 2.2, morphometric interpretation in Section 2.3, and finally we demonstrate properties for optimization in Section 2.4.

2.1 Helmholtz Decomposition of Vector Fields - Introducing Two New Deformation Potentials

We define a warp function φ as the mapping between two 3-dimensional images, the image I and the reference R , $\varphi : \mathbb{R}^3 \rightarrow \mathbb{R}^3$, which satisfies that the point \mathbf{x} in the reference R corresponds to the point $\varphi(\mathbf{x})$ in the image I . The important aspect of this definition is that that φ can be considered a vector field. For medical image analysis purposes we can furthermore assume that the vector field is smooth, as this will usually be our best assumption for the anatomical topology. These considerations also holds for the deformation field, \mathbf{u} , which we define as the difference from the identity warp, such that $\varphi = \mathbf{x} + \mathbf{u}$.

We apply the Helmholtz decomposition to the deformation field, using the fact that a vector field, which is twice continuously differentiable and with rapid enough decay at infinity, can be split into a sum

of the gradient of a scalar function and the curl of a vector function (Griffith, 1999)

$$\mathbf{u}(\mathbf{x}) = \nabla V(\mathbf{x}) + \nabla \times \mathbf{A}(\mathbf{x}), \quad (1)$$

where $V : \mathbb{R}^3 \rightarrow \mathbb{R}$ and $\mathbf{A} : \mathbb{R}^3 \rightarrow \mathbb{R}^3$ are scalar and vector potentials functions respectively. Sections 2.2, 2.3 and 2.4 all deal with specific properties of this representation by potentials. Because they are new in the field of medical image analysis, we start by exploring some of the immediate properties of these potentials. Recall that the deformation field is merely a sum of the two, then we shall explore the gradient potential V , and the curl potential \mathbf{A} one at a time.

2.1.1 The Gradient Potential V

The gradient potential is roughly speaking governing local contraction or expansion, this is in particular true in the presence of sufficiently small deformations. The same potential is used in electrostatics to describe the electrical potential. In Figure 1 gradient potentials and their impact on the deformation field are illustrated. It can be observed how a positive versus a negative gradient results in expansion or contraction of the deformation fields. Two-dimensional functions are used for the purpose of illustration.

2.1.2 The Curl Potential \mathbf{A}

The curl potential field is the equivalent to the magnetic potential field in electrostatics. It is describing purely divergence-free deformations, which can be interpreted as vortices. In Figure 2 different curl potentials and their impact on the deformation field are illustrated. For the purpose of illustration only the z -component of the curl potential \mathbf{A} is illustrated, and only the impact on the x, y directions of the deformation field are illustrated.

2.2 Elastic Registration

As previously mentioned, the elastic potential is often used for image registration, which is often based on a physical motivation in terms of an elastic tissue model (Christensen et al., 1997; Kybic and Unser, 2003). Regularization is usually formulated by a potential \mathcal{S} and differential operators \mathcal{B} (Haber and Modersitzki, 2007)

$$\mathcal{S}[\mathbf{u}] = \int_{\Omega} \langle \mathcal{B}[\mathbf{u}], \mathcal{B}[\mathbf{u}] \rangle_{\mathbb{R}^d} d\mathbf{x} . \quad (2)$$

The corresponding Gâteaux derivative is then given by

$$d_{\mathbf{u};\mathbf{v}}\mathcal{S}[\mathbf{u}] = \int_{\Omega} \langle \mathcal{A}[\mathbf{u}](\mathbf{x}), \mathbf{v}(\mathbf{x}) \rangle_{\mathbb{R}^d} d\mathbf{x} , \quad (3)$$

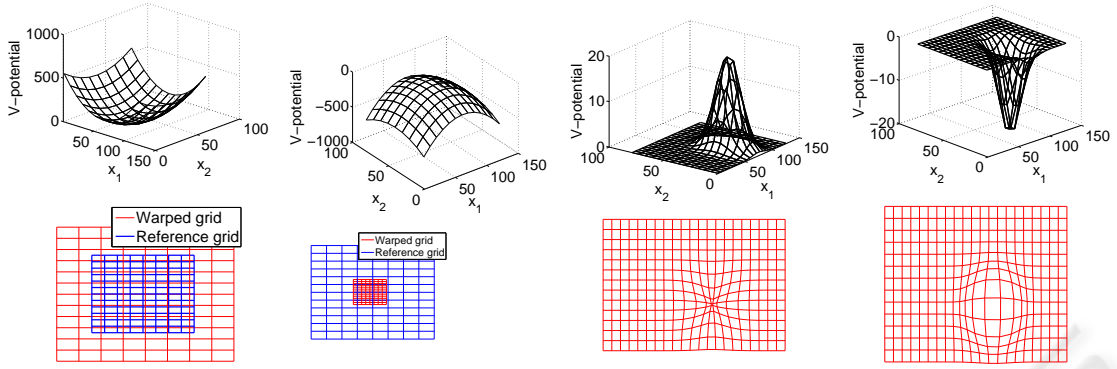


Figure 1: Gradient potentials, V , are illustrated in the upper row, and their impact on the deformation fields are shown below. The quadratic surfaces with constant curvature produce global scaling, and the potentials with local variations produce a local contraction or expansion.

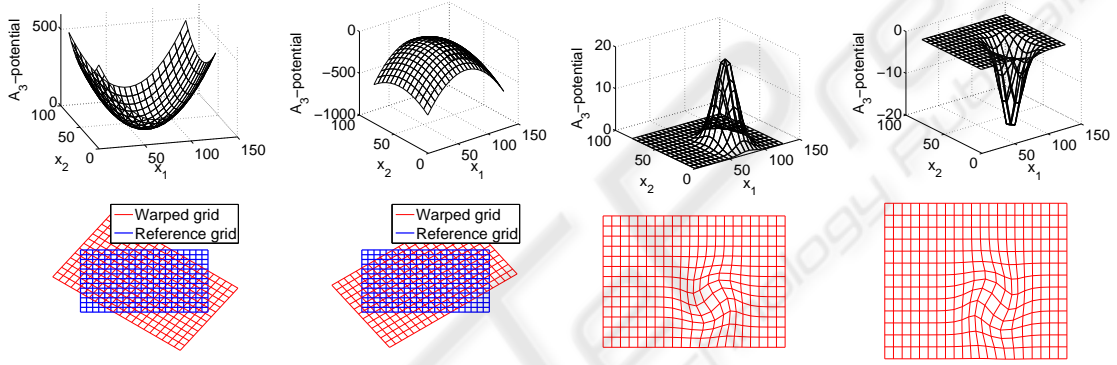


Figure 2: z -component, A_z of curl potential fields \mathbf{A} are shown in the upper row, and the impact on the x, y coordinates of the deformation field are shown below. A quadratic potential with constant curvature produces a global rotation of the deformation field, and a local change to the potential results in a local vortex in the deformation field.

where $\mathcal{A} = \mathcal{B}^* \mathcal{B}$. For the elastic potential this Navier-Lamé operator is given by

$$\mathcal{A} = \mathcal{B}^* \mathcal{B} [\mathbf{u}] = \mu \Delta \mathbf{u} + (\lambda + \mu) \nabla (\nabla \cdot \mathbf{u}) \quad (4)$$

2.2.1 Elastic Registration of the Helmholtz Decomposition

We examine how the elastic potential affects the Helmholtz decomposition of the warp field, and straightforward calculations give

$$\mathcal{P}[\mathbf{u}] = \int_{\Omega} \mu \sum_{a,b=1}^3 \varepsilon_{ab}^2 + (\mu + \lambda) (\nabla \cdot \mathbf{u})^2 dx, \quad (5)$$

where $\varepsilon_{ij} = \delta u_i / \delta x_j + \delta u_j / \delta x_i$. Now $\mathbf{u} = \nabla V + \nabla \times \mathbf{A}$ and

$$\begin{aligned} \mathcal{A}[\mathbf{u}] &= \mu \Delta \mathbf{u} + (\lambda + \mu) \nabla (\nabla \cdot \mathbf{u}) \\ &= \mu \Delta (\nabla V + \nabla \times \mathbf{A}) \\ &+ (\lambda + \mu) \nabla (\nabla \cdot (\nabla V + \nabla \times \mathbf{A})) \\ &= (2\mu + \lambda) \nabla \Delta V + \mu \Delta \nabla \times \mathbf{A}. \end{aligned} \quad (6)$$

This is a rather remarkable result, since we can now decouple the two potentials. Let $\lambda_1 = 2\mu + \lambda$ and $\lambda_2 = \mu$, then

$$\mathcal{A}[\mathbf{u}] = \lambda_1 \nabla \Delta V + \lambda_2 \Delta \nabla \times \mathbf{A} \quad (7)$$

and replacing the Lamé constants μ and λ by λ_1 and λ_2 , we have a clear notion of how to interpret the two regularization parameters. Not all values of λ_1 and λ_2 have meaning in a physical material-property sense (as goes for a negative μ as well), which should be considered. It can be argued, though, that the computational model should be extended to include these cases as well (Modersitzki, 2004). All derivations are also valid if we had differentiated in the time-domain, so our potential representation has the same advantages in fluid image registration.

2.3 Deformation-based Morphometry

Following Chung *et al.* we shall assume that the displacement field \mathbf{u} is a smooth function in time, capturing the variation in shape over time (Chung *et al.*,

2001). In Section 3 we discuss how an artificial time can be introduced, even when we are doing inter-subject registration. Introducing deformation fields as a function of time, $\mathbf{u}(\mathbf{x}, t)$, the deformation field \mathbf{u} at $\mathbf{x} + d\mathbf{x}$ can be written using a Taylor expansion

$$\mathbf{u}(\mathbf{x} + d\mathbf{x}, t) \approx \mathbf{u}(\mathbf{x}, t) + \mathbf{J}_u d\mathbf{x}, \quad (8)$$

where \mathbf{J}_u denotes the Jacobian of the deformation field. It is usually assumed that the Jacobian contains all information relevant in morphometry, and still following Chung we shall look at a possible decomposition of it.

2.3.1 Vorticity and Strain of the Jacobian

The Jacobian can be divided into symmetric and anti-symmetric parts by the following decomposition

$$\frac{\partial u_j}{\partial x_i} = \frac{1}{2} \left(\frac{\partial u_j}{\partial x_i} - \frac{\partial u_i}{\partial x_j} \right) + \frac{1}{2} \left(\frac{\partial u_j}{\partial x_i} + \frac{\partial u_i}{\partial x_j} \right) \quad (9)$$

The first antisymmetric part is termed vorticity and the second part the strain. Using this (8) may be written as

$$\mathbf{u}(\mathbf{x} + d\mathbf{x}, t) = \mathbf{u}(\mathbf{x}, t) - \frac{1}{2} \nabla \times \mathbf{u}(\mathbf{x}, t) \times d\mathbf{x} + \boldsymbol{\epsilon}(\mathbf{x}, t) d\mathbf{x}, \quad (10)$$

where the strain matrix is given by $\boldsymbol{\epsilon} = (\epsilon_{ij}) = \frac{1}{2} \left(\frac{\partial u}{\partial \mathbf{x}} + \left(\frac{\partial u}{\partial \mathbf{x}} \right)^T \right)$. Observe that the vorticity depends on the \mathbf{A} potential alone. Since $\nabla \times \nabla V(\mathbf{x}, t) = 0$ we get $\nabla \times \mathbf{u}(\mathbf{x}, t) = \nabla \times \nabla \times \mathbf{A}(\mathbf{x}, t)$. The diagonal elements of the strain matrix $\boldsymbol{\epsilon}$ are in particular given by

$$\begin{aligned} \epsilon_{11} &= \frac{1}{2} \left(\frac{\partial u_1}{\partial x_1} + \frac{\partial u_1}{\partial x_1} \right) \\ &= \frac{\partial \left(\frac{\partial A_2}{\partial x_3} - \frac{\partial A_3}{\partial x_2} + \frac{\partial V}{\partial x_1} \right)}{\partial x_1} \end{aligned} \quad (11)$$

Taking the temporal derivative, the deformation velocity can be written as

$$\begin{aligned} \frac{\partial \mathbf{u}(\mathbf{x} + d\mathbf{x}, t)}{\partial t} &= \frac{\partial \mathbf{u}(\mathbf{x}, t)}{\partial t} \\ &\quad - \frac{1}{2} \frac{\partial}{\partial t} \nabla \times \mathbf{u}(\mathbf{x}, t) \times d\mathbf{x} + \frac{\partial \boldsymbol{\epsilon}(\mathbf{x}, t) d\mathbf{x}}{\partial t} \end{aligned} \quad (12)$$

and in (Chung et al., 2001) it is shown that the first order approximation to the Jacobian determinant is the sum of the diagonal elements of the strain matrix $\boldsymbol{\epsilon}$;

$$\begin{aligned} \frac{\partial |\mathbf{J}_u|}{\partial t} &\approx \frac{\partial \epsilon_{11}}{\partial t} + \frac{\partial \epsilon_{22}}{\partial t} + \frac{\partial \epsilon_{33}}{\partial t} = \\ &\quad \frac{\partial}{\partial t} \left(\frac{\partial^2 V}{\partial x_1^2} + \frac{\partial^2 V}{\partial x_2^2} + \frac{\partial^2 V}{\partial x_3^2} \right). \end{aligned} \quad (13)$$

This is seen to depend on the gradient potential alone, which can be understood, when we consider that this approximation of the Jacobian determinant is the divergence of the deformation field, $\nabla \cdot \mathbf{u}$. In summary we notice that our introduced representation gives several simplifications in relating our parameters to the morphological changes.

2.4 On Stability and Optimization

Hsiao *et al.* were using the curl and the divergence of the deformation field as parameters for image registration. Their experimental results showed this gave better stability in terms of avoiding grid folding than using a uniform B-spline parameterization (Hsiao et al., 2008). In the current setting these quantities are given by $\nabla \times \mathbf{u} = \nabla \times \nabla \times \mathbf{A}$ and $\nabla \cdot \mathbf{u} = \nabla \cdot \nabla V = \Delta V$ respectively. The div-curl solver presented could be applied for our parameterizations as well, disregarding that we are presenting a different regularization term. However, for the morphometry test in Section 3 we have applied a parameterized variational approach described in Appendix 4, which demonstrates our method with elastic regularization. We believe that the method presented in the current work has a number of advantages. They have to make use of inversions of discretized operators to reconstruct the actual deformation field in the optimization step, which gives them a registration less prone to folding. We can simply use the exact differential operators on our potentials in order to arrive at actual deformations in our formulation, and use the regularization to enforce smoothness and invertibility.

3 RESULTS

To demonstrate that the described parameterization can also be practically implemented, we have implemented a cubic B-spline parameterization of the two potential fields. The implementation is described in more detail in Appendix 4, and in the next section we show results, and hope to add more intuition for the presented approach through visualization of the potentials on 2D spaces.

3.1 Morphometry on Corpus Callosum

The corpus callosum has been the subject of much analysis in the field of medical imaging (Davatzikos et al., 1996; Rueckert et al., 2003). This is probably because of its relatively simple shape, and the good contrast in MRI. We have also chosen corpus callosum MR images sampled in the midsagittal plane to

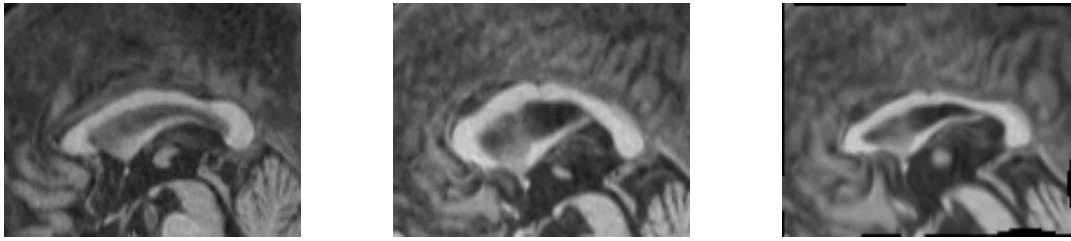


Figure 3: Registration by the proposed parameterization. The image in the middle is registered to the reference (left) and the result is shown to the right.

demonstrate the presented method. The data set used for the tests is a subset consisting of 62 MR images from the LADIS (Leukoaraiosis and DISability) study (Pantoni et al., 2005) - a pan-European study involving 12 hospitals and more than 700 patients. In the optimization we use an artificial time t , when registering one image to another (Modersitzki, 2004). Since the quantitative analysis is not the major objective of the current presentation, we put emphasis on illustrating properties of our potentials. In Figure 3 the image registration result of one corpus callosum to another is shown. We analyze the determinant of the deformation field to identify which areas are mostly deformed by the registration process. In Figure 4 the distribution of the determinant and the areas with significantly different values are illustrated. It is seen that the expansion (in this case) is most outspoken in 3 regions of the corpus callosum, which is not so surprising when we investigate the reference, and target image in Figure 3.

The potentials parameterizing the image registration are shown in Figure 5. It can be seen that the V -field is describing expansion and contractions, and several of the areas with interesting Jacobian determinant in Figure 4 are also seen to represent a rather strong contraction from the V -potentials. The A -field is describing rotation - or vortices in the deformation field.

4 DISCUSSION AND CONCLUSIONS

In this paper we introduce the theory of a new parameterization of 3D deformation fields to the field medical image analysis, using potentials and Helmholtz decomposition. Similar methods have already proven valuable in electrostatics and fluid flow estimation (Griffith, 1999; Kohlberger et al., 2003). We show the representation can be considered a natural parameterization for both elastic and fluid image registration due to the decoupling of the parameters. For mor-

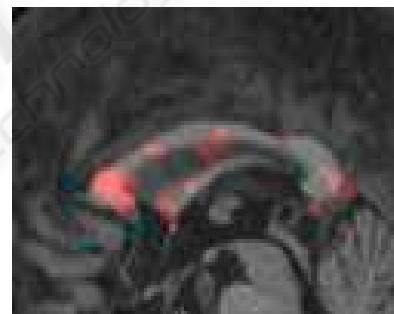
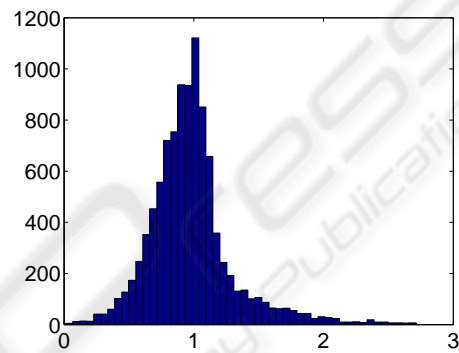


Figure 4: Above: The distribution of the determinant of the Jacobian. Below: Region of interest, where the deformation measured by the determinant, is outside a range of 2 std. dev..

phometry we have demonstrated that one of the two potentials directly gives us the vorticity of the deformation field. The determinant gradient field is shown to be the first-order small-deformation approximation to the determinant of the Jacobian matrix - probably the most accepted morphometry measure used. Contemporary methods for optimization can supposedly be adapted to the parameterization (Hsiao et al., 2008; Kohlberger et al., 2003) and we have outlined our implementation based on finite differences, in Appendix 4.

The major contribution of the paper is primarily a theoretical one, but we have for demonstration purposes included 2D examples illustrating the relation

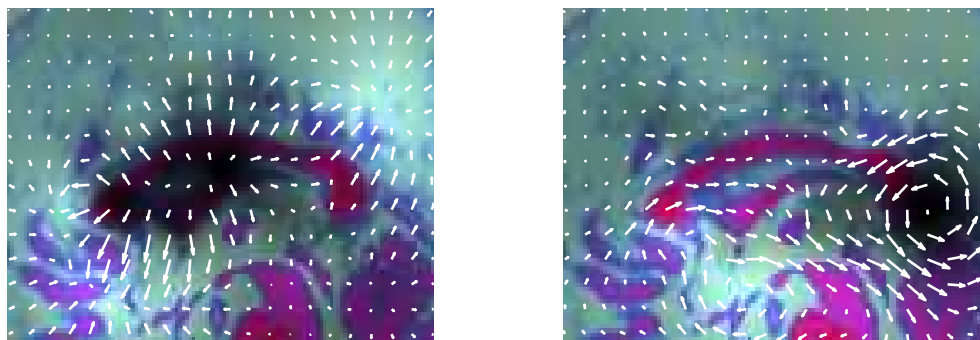


Figure 5: Potential functions shown with images and deformation fields using the HSV colormap. The potential is the value and the image is the hue. Left: V -potential along with (normalized) deformations this potential causes. Right: A -potential, and the curl deformations this potential causes.

between the potentials and the observed deformation fields. It is shown that we can get sensible results, where most of the theoretical observations are readily recognizable from our empirical experiments, and we anticipate many applications in the field of morphometry. For future work we plan to design quantitative tests on different medical data sets, to add further empirical validation to the theoretic results demonstrated in the current paper, and to document the impact on achieved solutions.

REFERENCES

- Christensen, G. E., Joshi, S. C., and Miller, M. I. (1997). Volumetric transformation of brain anatomy. *IEEE Trans. Med. Imag.*, 16(6):864–877.
- Chung, M. K., Worsley, K. J., Paus, T., Cherif, C., Collins, D. L., Giedd, J. N., Rapoport, J. L., and Evans, A. C. (2001). A unified statistical approach to deformation-based morphometry. *NeuroImage*, 14 (3):595–606.
- Cootes, T., Twining, C., and Taylor, C. (2004). Diffeomorphic statistical shape models. *British Machine Vision Conference*, 1:447–456.
- Davatzikos, C., Vaillant, M., Resnick, S., Prince, J., Letovsky, S., and Bryan, R. (1996). A computerized approach for morphological analysis of the corpus callosum. *J. Comput Assist Tomogr*, 20:88–97.
- Griffith, D. (1999). An introduction to electrodynamics. *Prentice Hall*.
- Haber, E. and Modersitzki, J. (2007). Image registration with a guaranteed displacement regularity. *International Journal on Computer Vision*, 71:361–372.
- Hsiao, H., Chen, H., Lin, T., Hsieh, C., Chu, M., Liao, G., and Zhong, H. (2008). A new parametric nonrigid image registration work based on helmholtz's theorem. *SPIE Symposium on Medical Imaging 2008*.
- Joshi, S. (1997). Large deformation diffeomorphisms and gaussian random fields for statistical characterization of brain sub-manifolds. *PhD thesis, Sever institute of technology, Washington University*.
- Kohlberger, T., Étienne Mémin, and Schnörr, C. (2003). Variational dense motion estimation using the helmholtz decomposition. *4th International Conference, Scale Space 2003*, 2695:980.
- Kybic, J. and Unser, M. (2003). Fast parametric elastic image registration. *IEEE Transactions on Image Processing*, 12(11):1427–1442.
- Modersitzki, J. (2004). Numerical methods for image registration. *Oxford Uni. Press*.
- Pantoni, L., Basile, A. M., Pracucci, G., Asplund, K., Bogousslavsky, J., Chabriat, H., Erkinjuntti, T., Fazekas, F., Ferro, J. M., Hennerici, M., O'Brien, J., Scheltens, P., Visser, M. C., Wahlund, L. O., Waldemar, G., Wallin, A., and Inzitari, D. (2005). Impact of age-related cerebral white matter changes on the transition to disability - the LADIS study: Rationale, design and methodology. *Neuroepidemiology*, 24(1-2):51–62.
- Rueckert, D., Frangi, A. F., and Schnabel, J. A. (2003). Automatic construction of 3D statistical deformation models of the brain using nonrigid registration. *IEEE Transactions on Medical Imaging*, 22(8):1014–25.
- Studholme, C. and Cardenas, V. (2007). Population based analysis of directional information in serial deformation tensor morphometry. *Medical Image Computing and Computer-Assisted Intervention - MICCAI 2007*, 4792:311–318.
- Vemuri, B. C., Yea, J., Y. Chen, b., and Leonard, C. M. (2003). Image registration via level-set motion: Applications to atlas-based segmentation. *Medical Image Analysis*, 7(1):1–20.

APPENDIX

In this section we give an overview of implementation details that are not of great importance to the theoretical contributions of this paper. In Section 4 we introduce the uniform cubic B-spline that are used in

our implementation. In Section 4 we show some details on their regularization, and in Section 2.4 we give some details on how the evaluations can be sped up.

B-spline Representation of Fields

We represented the potential fields by cubic B-splines, following (Rueckert et al., 2003). So in summary the two potential fields are represented as

$$V = \sum_{k=0}^3 \sum_{l=0}^3 \sum_{m=0}^3 B_k(r)B_l(s)B_m(t)v_{k,l,m} \quad (14)$$

$$\mathbf{A} = \sum_{k=0}^3 \sum_{l=0}^3 \sum_{m=0}^3 B_k(r)B_l(s)B_m(t)\mathbf{a}_{k,l,m} \quad (15)$$

Regularization of the B-splines

Applying the elastic constraints (6) to the B-spline fields, we get for the scalar potential

$$\begin{aligned} \nabla \Delta V = \nabla \sum_{k,l,m=0}^3 (B_k''(r)B_l(s)B_m(t) \\ + B_k(r)B_l''(s)B_m(t) + B_k(r)B_l(s)B_m''(t))v_{k,l,m} \end{aligned} \quad (16)$$

and for the vector potential we get

$$\begin{aligned} \Delta \nabla \times \mathbf{A} = \\ \Delta \nabla \times \sum_{k=0}^3 \sum_{l=0}^3 \sum_{m=0}^3 B_k(r)B_l(s)B_m(t)\mathbf{a}_{k,l,m} \end{aligned} \quad (17)$$

The regularization of the control points is now determined by

$$\begin{aligned} \frac{\delta S[\mathbf{u}]}{\delta v_{lkm}} = d_{\mathbf{u}, \frac{\delta \mathbf{u}}{\delta v_{lkm}}} S[\mathbf{u}] = \\ \int_{\Omega} \left\langle \mathcal{A}[\mathbf{u}](\mathbf{x}), \frac{\delta \mathbf{u}}{\delta v_{lkm}} \right\rangle d\mathbf{x} \end{aligned} \quad (18)$$

Optimization

We note that in our parameterized setting, the \mathcal{A} -operator can be written as linear combination of the parameters $\mathcal{A} = K_{\mathcal{A}}\mathbf{p}$, as can the warp field $\mathbf{u} = K_{\mathbf{u}}\mathbf{p}$. Using this (18) can be rewritten as

$$\begin{aligned} \frac{\delta S[\mathbf{u}]}{\delta v_{lkm}} = d_{\mathbf{u}, \frac{\delta \mathbf{u}}{\delta v_{lkm}}} S[\mathbf{u}] = \\ \int_{\Omega} (K_{\mathcal{A}}\mathbf{p})^T K_{\mathbf{u},klm} d\mathbf{x} = \mathbf{p}^T \int_{\Omega} K_{\mathcal{A}}^T K_{\mathbf{u},klm} d\mathbf{x} \end{aligned} \quad (19)$$

it is seen that the Gateaux derivative is indeed linear in the parameters, and the integral needs only be evaluated once. The distance measure between reference and image can for instance be the L_2 -norm

$$\mathcal{D}[R, T; \mathbf{u}] = \int_{\Omega} [T(x + \mathbf{u}) - R(x)]^2 dx \quad (20)$$

with the Gateaux derivative

$$d_{\mathbf{u}; v} \mathcal{D}[R, T; \mathbf{u}] = \int_{\Omega} \langle \mathbf{f}(x, \mathbf{u}(x)), \mathbf{v} \rangle_{R^d} dx$$

where $\mathbf{f}(x, \mathbf{u}(x))$

$$= \nabla T(x + \mathbf{u}(x))(T(x + \mathbf{u}(x)) - R(x)) \quad (21)$$

And the same kernel substitutions can be made as for the regularization. This facilitates a quick estimation of the deformation field. A further speed up is gained by implementing a multi-grid cubic B-spline approach has been used, which also helps avoid local minima. In our presented results we used control point distances of 5, 10 and 20 pixels, respectively.